Opto-Electronic Advances

Soft chiral superstructure enabled dynamic polychromaticholography

Chun-Ting Xu†, Lu Li†, Quan-Ming Chen, Guang-Yao Wang and Wei Hu*

https://doi.org/10.29026/oea.2026.250177

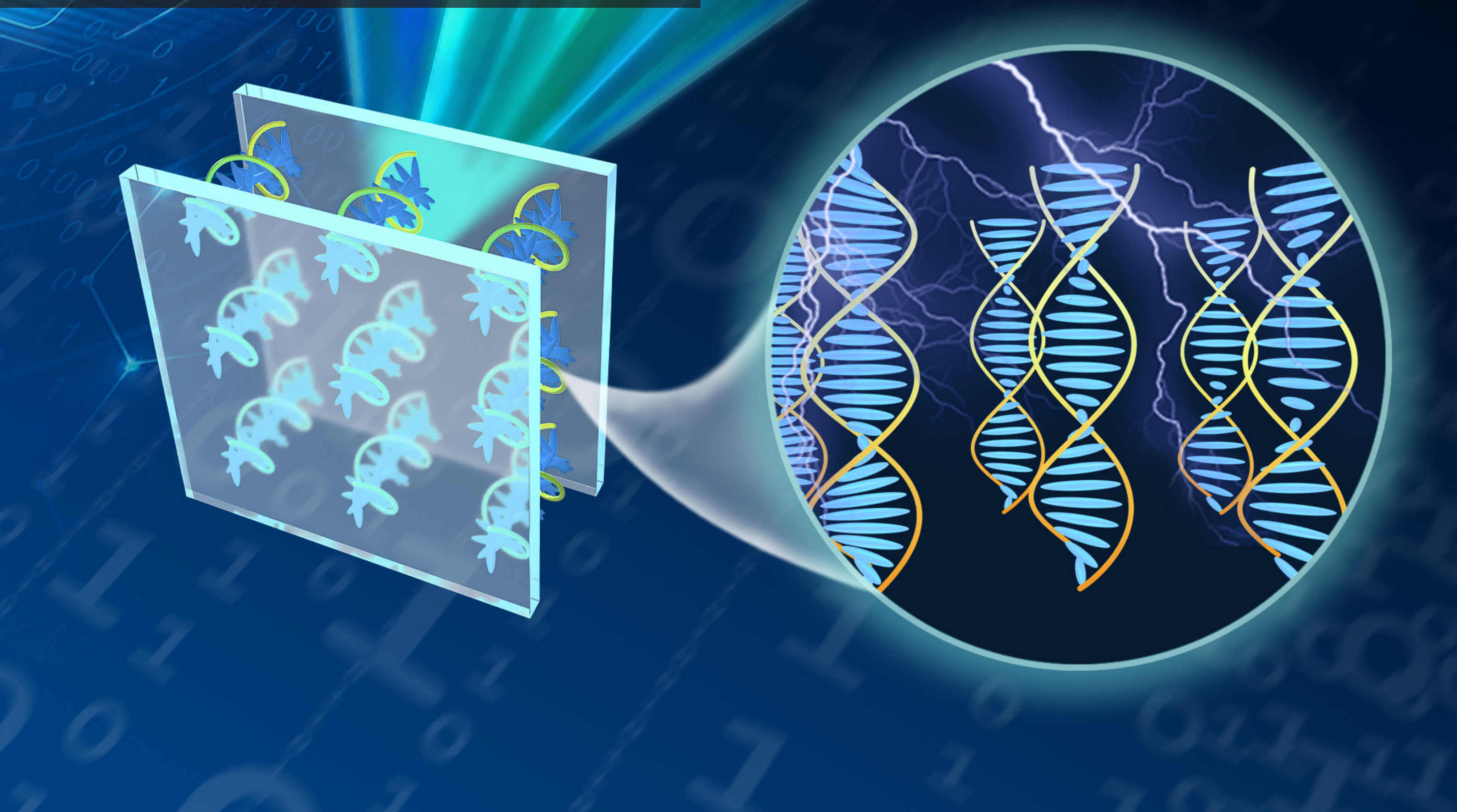

OEA | Opto-Electronic Advances

CN 51-1781/TN ISSN (Print) 2096-4579 ISSN (Online) 2097-3993

Soft chiral superstructure enabled dynamic polychromatic holography

Chun-Ting Xu, Lu Li, Quan-Ming Chen, Guang-Yao Wang and Wei Hu*

Citation: Xu CT, Li L, Chen QM et al. Soft chiral superstructure enabled dynamic polychromatic holography. *Opto-Electron Adv* **9**, 250177 (2026).

https://doi.org/10.29026/oea.2026.250177

Received: 3 July 2025; Accepted: 26 November 2025; Published online: 22 January 2026

OEA | Opto-Electronic Advances

Article

February 2026, Vol. 9, No. 2

Open Access

Soft chiral superstructure enabled dynamic polychromatic holography

Chun-Ting Xu[†], Lu Li[†], Quan-Ming Chen, Guang-Yao Wang and Wei Hu*

Abstract: Planar optics offers a compact and versatile platform for manipulating multiple dimensions of light parameters and thus has attracted tremendous interest in high-density data storage, high-security information encryption, and holographic displays. It is still challenging to achieve active functionalities via dynamically operating light-matter interactions inside these planar optics. Here, a polymer-stabilized cholesteric liquid crystal (CLC) is adopted as a tunable one-dimensional chiral superstructure. The bandgap tends to change from a periodic helix to a gradient-pitch configuration under direct current (DC) voltage, and the reflection bandwidth varies from a narrow band of 40 nm to a broad band of 180 nm. Off-axis phase-only holograms of three primary colors are properly *k*-space engineered via a modified Gerchberg-Saxton algorithm, and recorded into the initial alignments of the CLC by photopatterning. By altering the applied DC voltage, the generated holography actively switches between a monochromatic and polychromatic image. Moreover, spin-selective Bragg-Berry phase encoding in photopatterned superstructures with opposite helicity allows distinct holograms (e.g., "weather sign" and "chameleon") to be independently generated and modulated. This work takes full advantage of soft chiral superstructures for on-demand light control and has great potential in dynamic holography, information encryption, and data storage.

Keywords: polychromatic holography; cholesteric liquid crystals; polymer stabilization; geometric phase; photoalignment

DOI: 10.29026/oea.2026.250177 | CSTR: 32247.14.oea.2026.250177

Citation: Xu CT, Li L, Chen QM et al. Soft chiral superstructure enabled dynamic polychromatic holography. *Opto-Electron Adv* **9**, 250177 (2026).

1 Introduction

Multiple dimensions of light, such as phase, wavelength, and polarization, can be regarded as separate information carriers, enhancing the capacity of data transmission, processing, and display. Currently, the multiplexing and dynamic modulation of multiple optical parameters are highly pursued in vital fields, including optical communications, data storage, and holographic displays. Recently, planar optics formed by metasurface[1–3] et al. have broken the dependency of traditional optical elements on propagation phase accumulation and offer a compact platform for light modulation that significantly promotes the development of ultrathin planar optics. Metasurfaces can freely modulate multiple parameters of light by tailoring the geometric parameters or long-axis orientations of metal or dielectric meta-atoms[4–8]. However, their functions are often static and lack of tunability once fabricated. To release dynamic functions, chiral metasurfaces[9] or heterogeneous integration with active materials such as phase change materials[10], two-dimensional materials[11], micro-electro-mechanical systems[12], semiconductors[13], and liquid crystals (LCs)[14] have been adopted. Exploiting new mechanisms and technologies for active planar optics remains an urgent pursuit.

LC has been proven to be a perfect candidate for spatial light modulation. On the one hand, its electro-optical tunability enables instant modulation of the propagation phase; on the other hand, arbitrary geometric phases can be directly encoded to its local azimuthal orientation[15–19]. In recent years, impressive progress has been made in LC-based

Received: 3 July 2025
Accepted: 26 November 2025
Published online: 22 January 2026

National Laboratory of Solid State Microstructures, Key Laboratory of Intelligent Optical Sensing and Manipulation, and College of Engineering and Applied Sciences, Nanjing University, Nanjing 210023, China.
[†]These authors contributed equally to this work.
*Correspondence: W Hu, E-mail: huwei@nju.edu.cn

multidegree optical modulation, which takes advantage of self-organized hierarchical structures of LCs to independently modulate multiple degrees of light[20,21]. Among various categories, cholesteric liquid crystals (CLCs) have garnered significant attention because of their distinctive one-dimensional chiral photonic crystal characteristics[22–24]. It enables spin-selective and broadband-equal-efficiency Bragg-Berry phase modulation for wavelengths within the photonic bandgap (PBG)[25–27]. When the helical pitch of the CLC is tuned by external fields, including stress, heat, humidity, light and electricity, the PBG is adjusted accordingly[28]. It releases the freedom of working wavelength manipulation and thus facilitates applications in sensors, active color filters, reflective displays, and tunable mirrorless lasers[29–32]. Holography is carried out through modulating the wavefront of light and is promising for data storage, encryption, and information display[33–38]. All the information is recorded or reconstructed into the structure of the optical media. With the explosive growth of information, efforts toward multichannel modulation have been made to increase the transmission capacity[39–43]. A polychromatic and dual-spin hologram is reported by stacking six discrete CLC polymer films encoded with different patterns for separate wavelengths and spins[39]. Both heat- and electric-driven dynamic vectorial polychromatic holography is demonstrated in a bi-chiral wash-out-refill CLC[40]. Heliconical CLCs and inversely designed metasurfaces are combined to separately modulate the spectral and spatial functions simultaneously[41]. The above multiplexing methods still suffer from precise alignment, constrained working bands, or complicated fabrication. Therefore, it is imperative to develop new planar optics with dynamic and multichannel functions.

In this work, we propose dynamic polychromatic holography based on the programming of a polymer-stabilized chiral superstructure. Proper off-axis and phase-only holograms are designed via a modified Gerchberg-Saxton (GS) algorithm based on a *k*-space engineering technique, and then they are encoded into the initial orientations of CLCs to preprogram the image synthesis. Along with the working bandwidth tuned from 40 nm to 180 nm via continuously increasing the applied direct current (DC) voltage, the generated holographic image is actively switched from a monochromatic image to an RGB-polychromatic image. The reverse process occurs when the voltage decreases within several hundred milliseconds. Leveraging the spin-selective Bragg-Berry phase encoding of CLCs, distinct holograms are generated through alternating the incident circular polarization with cascaded CLCs of opposite helicity recorded with separate information. This work offers switchable multichannel holography tuned by working bandwidths and incident spins. It unlocks the potential of chiral CLC planar optics and may inspire innovative applications in dynamic polychromatic holography, high-security anticounterfeiting, and high-density data storage.

2 Design and principle of dynamic polychromatic holography

Similar to the geometric phase modulation of the nematic LC, the Bragg-Berry phase of the CLC also arises from the spin-orbit coupling of the selectively reflected light. Notably, for the latter case, only circularly polarized light of the same handedness as the CLC helix and wavelengths within the PBG is encoded with the designed phase. The residual light directly transmits the CLC and has a uniform phase delay. The Bragg reflection band is defined by n_oP–n_eP, where n_o/n_e represent ordinary/extraordinary refractive indices, and P is the helical pitch. Consequently, the central wavelength is $\lambda_c = (n_o + n_e)/2 \times P$, and the bandwidth is $\Delta\lambda = \Delta n \times P$, where Δn is the birefringence. The phase φ is recorded in the initial LC orientation of the helical superstructure α. The relationship between them is depicted by $\varphi = \pm 2\alpha$, where the sign is determined by the handedness of the CLC. The above lays the foundation for spin-selective wavefront modulation for orthogonal spins with photopatterned CLC of opposite helicity.

To achieve polychromatic holography via wavelength multiplexing, the holographic pattern is designed via a *k*-space engineering technique with a modified GS algorithm (Supplementary information of Section 1). By encoding different holograms into separate cascaded chiral superstructures of opposite helicity, different polychromatic diffraction patterns (weather signs and a chameleon) can be obtained for orthogonal circular polarizations (Fig. 1(a)). Notably, to avoid size discrepancies in the far field, the holograms are optimized in the design. The red (R), green (G), and blue (B) components of the target are extracted and scaled. Subsequently, phase profiles φ_R, φ_G, and φ_B with respect to R, G, and B are calculated via the GS algorithm. Finally, after assigning proper phase shifts $\Delta\varphi_R$, $\Delta\varphi_G$, and $\Delta\varphi_B$ to φ_R, φ_G, and φ_B, the phase-only hologram is generated by multiplexing them in an amplitude ratio of C_R: C_G: C_B. The designed LC orientation is obtained through the following formula:

$$\alpha = \frac{1}{2}\arg\left(C_R e^{i\left(\varphi_R+\Delta\varphi_R\right)} + C_G e^{i\left(\varphi_G+\Delta\varphi_G\right)} + C_B e^{i\left(\varphi_B+\Delta\varphi_B\right)}\right). \tag{1}$$

As revealed in Fig. 1(b), distinct R, G, and B images are deflected toward predetermined angles, and the polychromatic image is reconstructed, as shown in the white dashed box marked zone. To realize dynamic tunability, we adopt a polymer-stabilized CLC with negative dielectric anisotropy ($\Delta\varepsilon < 0$). When a DC voltage is applied to the cell, the negative LC remains parallel to the glass substrate, whereas the electric field attracts the cations trapped in the polymer network to the cathode, causing the polymer to move toward the electrode[44]. Accordingly, LCs rearrange to form a helical structure of gradient pitch[45,46], which is depicted by

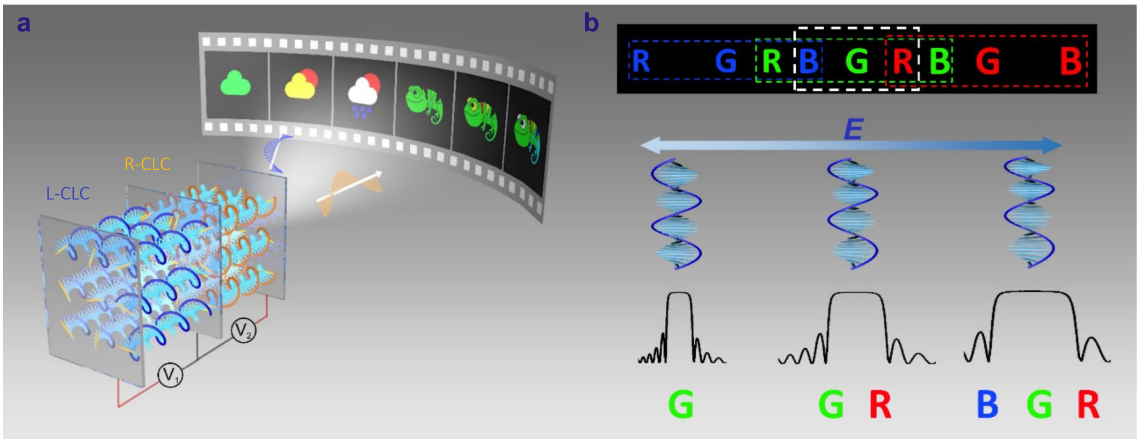

Fig. 1 | Schematic of dynamic polychromatic holography with wavelength and spin multiplexing. (a) Dynamic multichannel polychromatic holography based on cascaded chiral superstructures of opposite helicities and different initial orientations. The blue and yellow rods represent the LC director and SD1 orientations, respectively. The dark blue and orange springs surrounding the CLCs depict polymer networks of the same handedness as the CLCs. (b) Scheme for *k*-space engineered polychromatic holography. A polychromatic image of "BGR" is displayed in the white dashed box marked zone. Dependencies of spectra and observed letters on the evolution of chiral superstructures driven by DC voltage.

$$P(z) = P_0 + \frac{\partial P}{\partial z}(z - z_0), \quad (2)$$

where P_0 is the pitch at z_0, and z_0 is a characteristic position in the LC cell where $P(z_0) = P_0$[47]. The emergence of gradient pitch broadens the bandwidth and leads to variations in holographic images, as illustrated in Fig. 1(b). Moreover, dynamic spin- and wavelength-complexed polychromatic holography can be realized on cascaded chiral superstructures of opposite helicities and different initial orientations.

3 Results and discussion

The spectral variation under an electric field is characterized for a unidirectionally aligned polymer-stabilized CLC. At the beginning (E_0 = 0), the rod-like LC molecules rotate periodically along the helical axis, exhibiting a uniform helical pitch P_0. A narrow reflective band ($\Delta\lambda$ = 40 nm; λ_c = 560 nm) is measured for right circularly polarized (RCP) incidence (gray line in Fig. 2(a)). As the voltage increases to E_1 = 1.1 V/μm, the band gradually expands, as shown by the red line in Fig. 2(a). Finally, after the voltage increases to E_2 = 2.2 V/μm, the band covers a wide range from 470 nm to 650 nm (blue line in Fig. 2(a)). Band broadening is induced by the gradient pitch generated under DC voltage. A decrease in reflectance is observed during evolution, which is attributed to the reduction in pitch number. Notably, the device exhibits a remarkable fatigue resistance under the electric field switching (Fig. S9). Berreman's 4 × 4 matrix method[48] is further employed to calculate the variation in optical properties along with the evolution of chiral superstructures. Figure 2(b) shows that the simulated reflectance and Bragg-Berry phase are dependent on the wavelength and initial orientation angle of the helical superstructure in the voltage OFF and ON states. A narrow band reflection is obtained in the OFF state because of the uniform pitch, and the band significantly broadens in the ON state as the configuration changes to a gradient pitch (Supplementary information of Section 2). The simulation is consistent with the above experiments. Moreover, the simulated Bragg-Berry phase encoded to the reflected light is exactly twice the initial orientation angle of the CLC, i.e., φ = +2α. Thus, it enables an electrical switch on different colored holographic patterns.

The hologram of a "ginkgo leaf" is encoded to the polymer-stabilized CLCs to verify the electrochromic holography. The phase profile φ_{leaf} is calculated via the GS algorithm. Consequently, the initial CLC orientation α_{leaf} = 1/2φ_{leaf} is recorded into the cell by photopatterning. Figure 2(c) shows the calculated phase diagram and observed planar textures of the cell. With increasing applied electric field, the color of the CLC textures varies accordingly. The color purity gradually decreases due to broadening of the reflection band. Different colored far-field "ginkgo leaf" images are obtained with various incident wavelengths R (630 nm), G (550 nm), and B (480 nm) and electric fields. At 0 V/μm, a green "leaf" is obtained, whereas images for the R and B wavelengths are very weak. As the electric field increases, the red and blue "leaf" appear sequentially for monochromic incidence. For RGB polychromatic incidence, green, yellow and white leaves are subsequently observed. The central bright dots result from phase errors and mirror reflections. Excessive red or yellow edges are generated because the image size is positively correlated with the wavelength. This vividly verifies the transformation of the monochromic image to a polychromatic image as a result of bandwidth broadening.

By properly tailoring the ratio among three primary colors (R, G, B), all colors within the color triangle can be

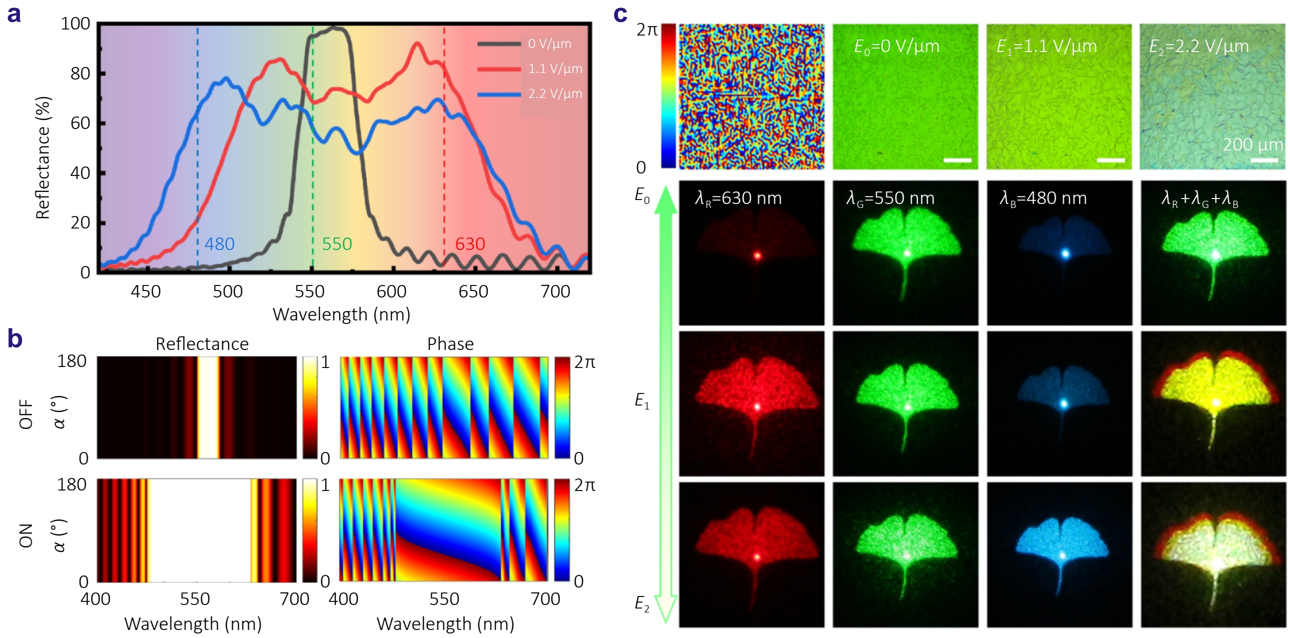

Fig. 2 | Electrochromic holography via polymer-stabilized CLCs. (a) Dependency of reflectance on wavelength with different DC voltages applied. The blue, green, and red dashed lines correspond to wavelengths of blue 480 nm, green 550 nm, and red 630 nm, respectively. (b) Simulated reflectance and Bragg-Berry phase dependence on the wavelength and initial orientation angle of the helical superstructure in the voltage OFF and ON states, respectively. The color bars indicate the reflectance and encoded phase, respectively. (c) The upper row images show the phase profile of a "ginkgo leaf" and corresponding LC textures observed under a POM at different voltages. The color bars indicate the phase. The bottom images show reconstructed holographic patterns for different incident wavelengths and applied voltages.

generated, which is fundamental to existing displays. Here, we select RGB as the basis for constructing color holographic images. As presented in Fig. 3(a), the phase-only off-axis hologram of "Flower and Butterfly" is generated, employing the modified GS algorithm that corrects both the size and position of the polychromatic components. The $\boldsymbol{k}$ relationship is depicted as $\boldsymbol{k}_{\text{out}} = -\boldsymbol{k}_{\text{in}} + \boldsymbol{k}_0$, where $\boldsymbol{k}_{\text{out}}$ and $\boldsymbol{k}_{\text{in}}$ denote the wavevectors of the output and input light, respectively, and $\boldsymbol{k}_0$ are externally introduced one by the tilt phase of the designed hologram. Correspondingly, the R, G, and B components are deflected to the desired angle in proper size and reassembled to form the designed polychromatic holography in a specific view zone. Figure 3(b) shows the simulated holographic images. In the white-dashed-box designated view zone, a "Flower and Butterfly" image with green "leaf", red "flower" and blue "butterfly" is obtained. By tuning the applied electric field, the image is switched between monochromatic and polychromatic holography.

Figure 3(c) illustrates the setup for characterizing the color holography. As revealed in Fig. 3(d), for E_0, only a green "leaf" is observed in the far field. The vibrant red "flower" and blue "butterfly" emerge at E_1 and E_2 subsequently because of the extension of the bandwidth. The experimental results are in good agreement with the simulation results (Fig. S10). Notably, the process is reversible, and all the images are of good quality and have low crosstalk (Supplementary information Video S1). The deflection angles and diffraction efficiencies of the RGB components are 7.6° and 19.6%, 6.6° and 17.5%, and 5.8° and 20.1%, respectively. The efficiency of G component is lower because that the anchoring effect of the middle layer is weaker than those adjacent to two substrates, leading to worse LC orientation. The calculated signal-to-noise ratios (SNRs) are 11.59 dB for R channel, 9.93 dB for B channel, and 11.92 dB for B channel, demonstrating the low crosstalk of our design. The response time for electrical switching is measured as well (Fig. 3(e)). The rise time, defined as the duration for the 10% to 90% normalized intensity change, of 658 ms is measured upon the application of E_2. Conversely, the fall time, representing 90% to 10% change, is recorded to be 331 ms after E removed. The experiments confirm the feasibility of fast switching of wavelength multiplexed polychromatic holography. The response times t_{R} and t_{F} of the polymer-stabilized CLC are expressed as follows[49]:

$$\begin{aligned} t_{\text{R}} &= \frac{\gamma_1}{\varepsilon_0 \left|\Delta\varepsilon\right| E^2 - k_{22}\pi^2/P^2} \\ t_{\text{F}} &= \frac{\gamma_1 P^2}{k_{22}\pi^2} \end{aligned}, \tag{3}$$

where γ_1 is the rotational viscosity of the LC and k_{22} is the twisted elastic constant. Thus, we can employ low-viscosity LC hosts to reduce the intrinsic resistance to molecular reorientation. Moreover, via introducing LC hosts with a larger negative $\Delta\varepsilon$, the dielectric torque significantly

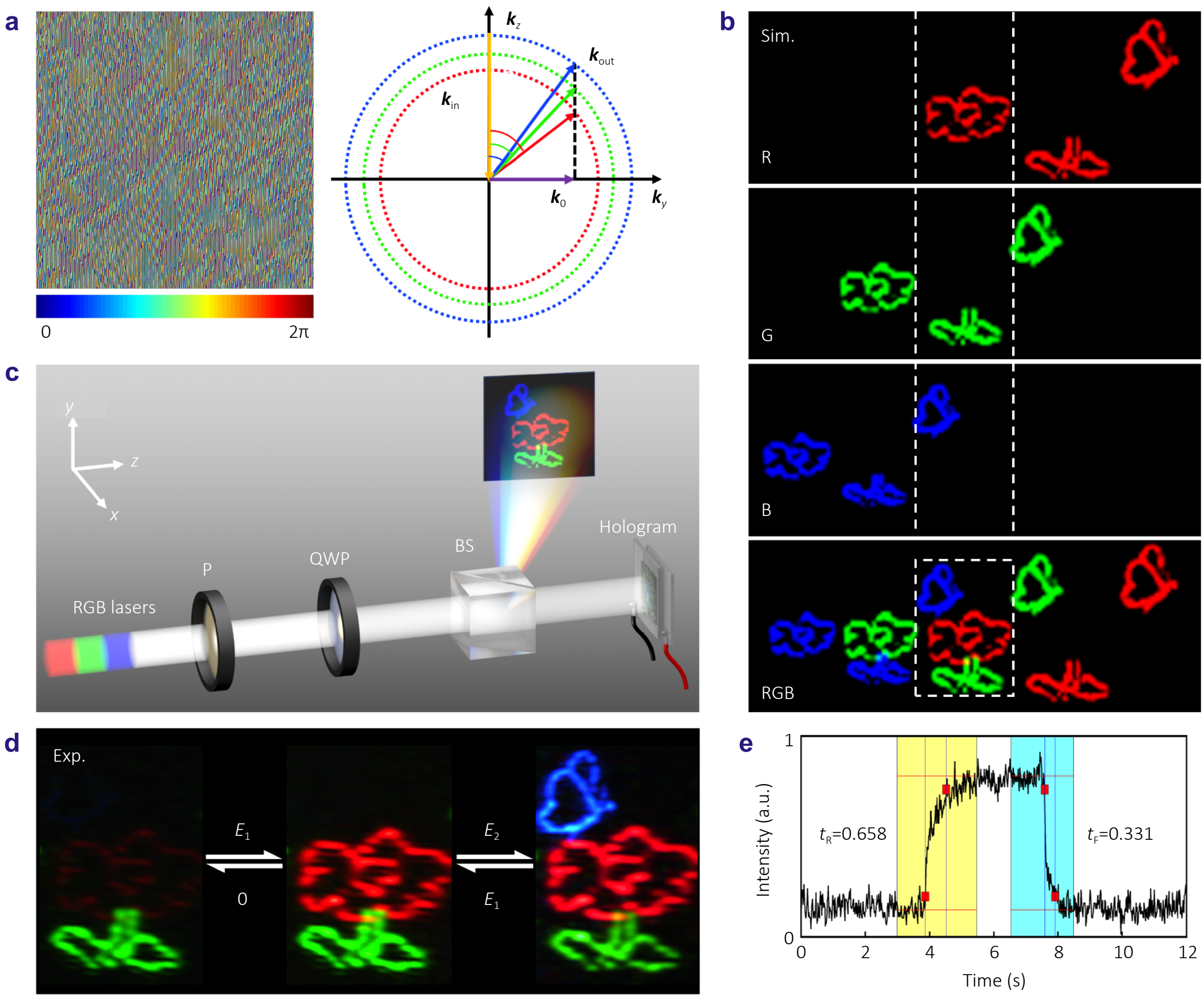

Fig. 3 | Wavelength-multiplexed polychromatic holography. (a) The left image represents the phase profile of the designed hologram. The right image shows the *k*-spacing engineering. The color bars indicate the designed phase. (b) Simulated holograms for RGB light incidence individually or simultaneously. (c) Experimental setup for characterizing polymer-stabilized CLC-based holography. P: polarizer; QWP: quarter waveplate; BS: nonpolarizing beam splitter. (d) Experimental results for simultaneous RGB incidence at different electric fields. (e) Response time measurement of the polymer-stabilized CLC-based holography.

increases, thus enables a stronger driving force for a given voltage, thereby accelerating the rise time.

The reflectance of the chiral superstructure exhibits a strong incident polarization dependency. As shown in Fig. 4(a), the lines/dots represent the theoretical/experimental spin-selective reflectances of left-handed CLC (L-CLC) and right-handed CLC (R-CLC), respectively. The degrees represent the angle between the transmission axis of the polarizer and the fast axis of the quarter waveplate. Both the experimental results and simulations validate the excellent spin selectivity of the reflectance. The slight difference between the experimental and theoretical results can be attributed to the polarization-independent Fresnel reflection from glass-air interface and a degree of polymer network scattering. On the basis of the inherent circular-polarization-selective geometric phase encoding of chiral superstructures, spin-complexed dynamic polychromatic holography is further demonstrated by cascading two polymer-stabilized CLC layers with opposite helicity. The configuration of the cascaded cell is illustrated in Fig. 4(b). The bottom layer is first photopatterned and filled with an R-CLC. After UV polymerization, the cell is photopatterned again to record the designed orientation of the second layer. Notably, the orientation of the R-CLC is maintained owing to polymer stabilization. Then, the L-CLC is filled, and a cascaded cell is finally obtained (Fig. S11).

On the basis of this cascaded cell, a hexa-channel switchable polychromatic holography is verified via the combination of spin and wavelength multiplexing. For a proof-of-concept demonstration, "weather signs" and "a chameleon" are selected as instances (target Ⅰ and target Ⅱ). As revealed in Fig. 4(c), for LCP incidence, a cloudy day sign, a sunny day sign, and a rainy-day sign appear sequentially with increasing *E*. Meanwhile, the cloud varies from green to

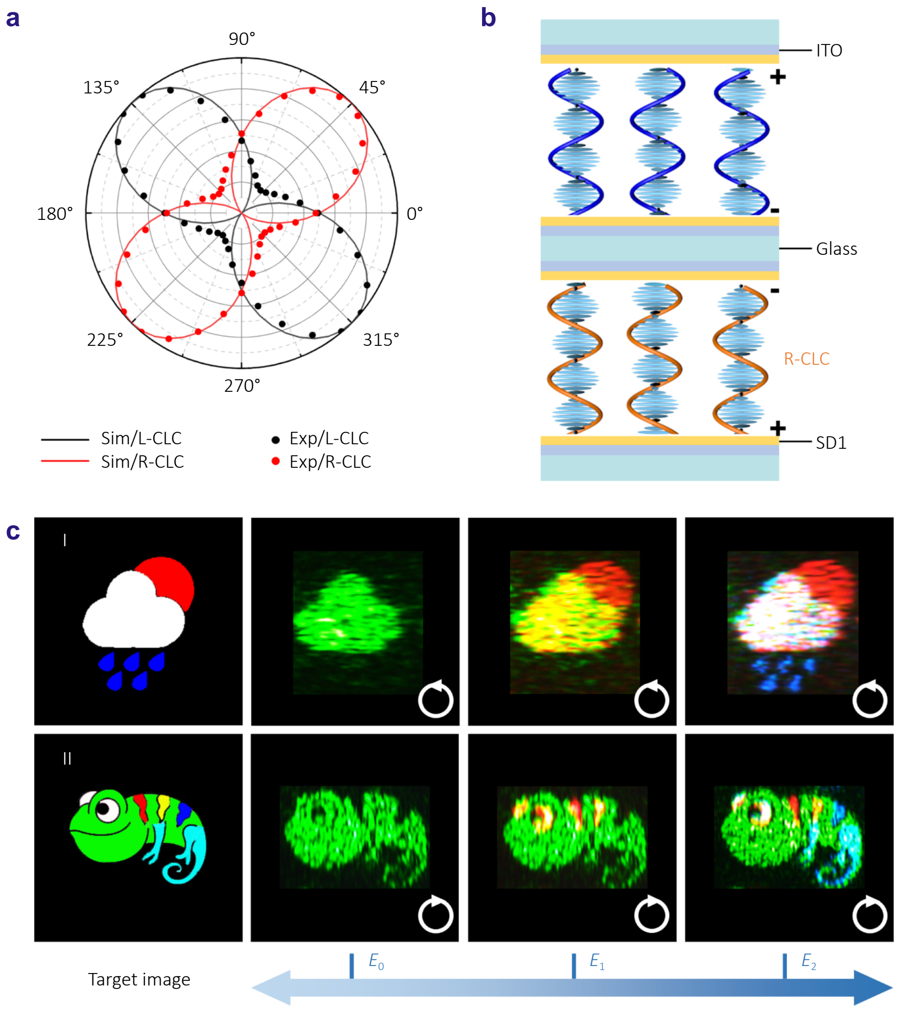

Fig. 4 | Spin-complexed dynamic polychromatic holography. (**a**) Spin-dependent diffraction efficiency of the sample. (**b**) Schematic illustration of cascaded opposite-chiral polymer-stabilized CLC. (**c**) Spin and wavelength multiplexed holography at different electric fields.

yellow and then to white due to color mixing. For RCP incidence, the color of the chameleon gradually changes from monochromatic to polychromatic with increasing *E*. Target Ⅰ and target Ⅱ can be selected by tuning the incident spins, while the color channels can be reversibly dropped or added by controlling the applied voltages.

The pursuit of polychromatic holography has been greatly advanced by metasurfaces, with techniques like *k*-space engineering pushing the limit of static device performance. However, the inherent static nature of these devices remains a significant bottleneck[50–52]. Our proposed wavelength- and spin-multiplexed polychromatic holography provides a versatile platform for dynamic and multiparameter spatial light modulation. The holographic phases can be freely recorded into the chiral superstructures via high-resolution photopatterning. A spatial resolution of up to 1.1 μm is achieved in the polymer-stabilized CLC based on the digital micromirror device (DMD)-based photopatterning system (Supplementary information of Section 3). Assuming the chiral superstructure is ideal, the largest achievable diffraction angle is 14.5°, which could be further enlarged by introducing more precise photoalignment techniques to achieve ultra-fine submicron period, including interference lithography and laser direct writing[53]. In our experiment, the diffraction efficiency of the polychromatic holography is ~20%, primarily resulting from polymer network scattering, non-ideal LC orientations, and reflection losses from glass substrates. Optimization of device configuration such as coating anti-reflection layers and introducing thicker cell gap could significantly improve the optical efficiency. With a cascaded cell of opposite helicity, switching between different predesigned holograms can be rapidly realized by altering the incident spins. Through electrically tuning the helical pitch of the chiral superstructure, wavelength channels can be reversibly dropped or added. The current response performance is adequate for applications where instantaneous switching is not critical. This includes static information displays and signage—such as holographic labels, art installations, and public information boards—where content updates are usually infrequent. Furthermore, it is highly suitable for optical encryption and anti-counterfeiting applications, where the color switching process enhances security.

In addition to the reflection mode, the strategy can be further adapted to transmission or even transflective mode by integrating nematic LCs and CLCs[54]. Additional dimensions of light can be added to increase the information capacity by introducing quasi-3D photonic crystals[20], vector holography[52], or orbital angular momentum holography[55,56]. Specifically, quasi-3D photonic crystals such as blue-phase LC with programmable defects enables control over the emission directionality of embedded fluorophores or lasing modes, thereby adding a propagation direction dimension to encoded information. Compared to scalar holography, LC vector holography possesses space-variant polarization states by engineering phases of left and right circularly polarized light, respectively. Thus, more distinct polarization channels can be selected by rotating the analyzer. Furthermore, spiral phase terms ($\exp(il\alpha)$, where l denotes topological charge) can be seamlessly incorporated into our design to achieve OAM holography, creating an orthogonal OAM multiplexing channel alongside wavelength and spin. The proposed dynamic holography can be applied in information encryption or optical camouflage. Specifically, the parameters for generating holographic images, including the wavelength, spin of light, and applied electric field, can be regarded as multiple security keys. The exact image can only be decrypted by using the predesignated keys, significantly enhancing the encryption security. In addition to holography, other dynamic functions, such as beam steering and imaging, can also be obtained through the proper design of orientation patterns.

4 Conclusions

We propose wavelength- and spin-multiplexed dynamic polychromatic holography based on photopatterned chiral superstructures. By tuning the applied voltage, on-demand holography from monochromatic to RGB-polychromatic cover of the entire visible spectrum is demonstrated. By means of k-space engineering based on the modified GS algorithm, electrically driven wavelength channel add and drop are realized as a single CLC element. Additionally, spin-complexed polychromatic holography with switchable hexa-channel functionalities is demonstrated with cascaded polymer-stabilized CLCs of opposite helicity. This work explores the capability of chiral soft matter in active spatial light modulation and may supply a compact, dynamic, and multi-channel platform that will trigger fantastic applications in dynamic holographic displays, beam shaping, information processing, and high-security encryption.

5 Experimental section

Materials: sulfonic azo-dye SD1 (NCLCP, China) is dissolved in dimethylformamide at a concentration of 0.3 wt.%. The spacer/glue mixture is composed of a 4% 8 μm spacer and 96% UV-curable glue. The initial polymerizable R-CLC/L-CLC mixture contains a nematic LC NC-M-LC708700-100 ($\Delta\varepsilon = -4.3$, $\Delta n = 0.092$; NCLCP, China), a right-handed/left-handed chiral dopant R5011/S5011 (NCLCP, China), a mesogenic monomer RM257 (NCLCP, China) and a photoinitiator diphenyl ketone (Shanghai Lingfeng Chemical Reagent Co. Ltd., China) at an optimized weight ratio of 88.52:2.48:8:1.

Sample fabrications: indium-tin-oxide glass substrates (1.5×2 cm^2) are treated by UV-ozone cleaning and then spin-coated with SD1 solution. Following an annealing process at 100 °C for 10 minutes, two substrates are assembled together and separated by an 8 μm spacer/glue mixture on both edges of one of them. Upon UV curing, an 8-μm-thick cell formed. A multistep-partly overlapping exposure is employed to record the designed orientation onto the CLC with a DMD-based photopatterning system (Fig. S5). The polymerizable CLC is then capillary filled into the cell at 100 °C. A 1 kHz AC square-wave signal at 5 V·μm^{-1} is applied across the cell for 1 minute to improve the uniformity of CLC orientations. Finally, the sample is exposed to a UV LED (365 nm; 30 mW·cm^{-2}) for 10 minutes to form the polymer-stabilized CLC (Fig. S6, S7).

Experimental measurements: the room temperature is 23.5 °C. The thermal range of 15–35 °C is feasible for polychromatic holography (Fig. S9). The reflection spectra are recorded via a spectrometer (PG2000-Pro, Ideaoptics, China). All the micrographs are captured under the reflective mode of a polarized optical microscope (Nikon 50i POL, Japan) with a pair of crossed polarizers. The electric field was output by a function generator (33522B, Agilent Technologies Inc., USA) and amplified by a voltage amplifier (2340, TEGAM, USA). RGB lasers are output simultaneously from a supercontinuum laser (SuperK EVO, NKT Photonics, Denmark) and selected with a multichannel acousto-optic tunable filter (SuperK SELECT, NKT Photonics, Denmark). The incident polarization is regulated by a polarizer and a quarter-wave plate. The reconstructed images are captured by a charge-coupled device (JCOPTIX, China). The intensity of the light is detected by a digital optical power meter (PM100D, Thorlabs, USA).

References

1. Yu NF, Genevet P, Kats MA et al. Light propagation with phase discontinuities: generalized laws of reflection and refraction. *Science* **334**, 333–337 (2011).
2. Sun SL, He Q, Xiao SY et al. Gradient-index meta-surfaces as a bridge linking propagating waves and surface waves. *Nat Mater* **11**, 426–431 (2012).
3. Deng QM, Li X, Hu MX et al. Advances on broadband and resonant

chiral metasurfaces. *npj Nanophoton* **1**, 20 (2024).
4. Zhao RZ, Huang LL, Wang YT. Recent advances in multi-dimensional metasurfaces holographic technologies. *PhotoniX* **1**, 20 (2020).
5. Xiong B, Liu Y, Xu YH et al. Breaking the limitation of polarization multiplexing in optical metasurfaces with engineered noise. *Science* **379**, 294–299 (2023).
6. Yin YY, Jiang Q, Wang HB et al. Multi-dimensional multiplexed metasurface holography by inverse design. *Adv Mater* **36**, 2312303 (2024).
7. Meng WJ, Fröch JE, Cheng K et al. Ultranarrow-linewidth wavelength-vortex metasurface holography. *Sci Adv* **11**, eadt9159 (2025).
8. Su H, Li BL, Bai YK et al. Achromatic 3D multi-color orbital angular momentum holography. *Adv Sci* **12**, 2503488 (2025).
9. Shi T, Deng ZL, Geng GZ et al. Planar chiral metasurfaces with maximal and tunable chiroptical response driven by bound states in the continuum. *Nat Commun* **13**, 4111 (2022).
10. Wang Q, Rogers ETF, Gholipour B et al. Optically reconfigurable metasurfaces and photonic devices based on phase change materials. *Nat Photonics* **10**, 60–65 (2016).
11. Li QS, Cai XD, Liu T et al. Gate-tuned graphene meta-devices for dynamically controlling terahertz wavefronts. *Nanophotonics* **11**, 2085–2096 (2022).
12. Manjappa M, Pitchappa P, Singh N et al. Reconfigurable MEMS Fano metasurfaces with multiple-input–output states for logic operations at terahertz frequencies. *Nat Commun* **9**, 4056 (2018).
13. Chen HT, Padilla WJ, Zide JMO et al. Active terahertz metamaterial devices. *Nature* **444**, 597–600 (2006).
14. Li SQ, Xu XW, Maruthiyodan Veetil R et al. Phase-only transmissive spatial light modulator based on tunable dielectric metasurface. *Science* **364**, 1087–1090 (2019).
15. Chen P, Wei BY, Ji W et al. Arbitrary and reconfigurable optical vortex generation: a high-efficiency technique using director-varying liquid crystal fork gratings. *Photonics Res* **3**, 133 (2015).
16. Wei BY, Chen P, Hu W et al. Polarization-controllable Airy beams generated via a photoaligned director-variant liquid crystal mask. *Sci Rep* **5**, 17484 (2015).
17. Luo ZY, Li YNQ, Semmen J et al. Achromatic diffractive liquid-crystal optics for virtual reality displays. *Light Sci Appl* **12**, 230 (2023).
18. Tang DL, Shao ZL, Xie X et al. Flat multifunctional liquid crystal elements through multi-dimensional information multiplexing. *Opto-Electron Adv* **6**, 220063 (2023).
19. Wang ZY, Zhou Z, Zhang H et al. Vectorial liquid-crystal holography. *eLight* **4**, 5 (2024).
20. Chen QM, Wang XY, Xu CT et al. Soft mesocrystal enabled multi-degree light modulation. *Laser Photonics Rev* **18**, 2301283 (2024).
21. Ouyang C, Chen QM, Xie ZY et al. Independent multiple-optical-parameter modulations enabled by manipulating the separate levels of a hierarchical structure. *Adv Opt Mater* **13**, 2402844 (2025).
22. Khoo IC, Wu ST, *Optics and Nonlinear Optics of Liquid Crystals* (World Scientific, Singapore, 1993).
23. Chen P, Wei BY, Hu W et al. Liquid-crystal-mediated geometric phase: from transmissive to broadband reflective planar optics. *Adv Mater* **32**, 1903665 (2020).
24. Chen QM, Xu CT, Liang X et al. Helical structure endows liquid crystal planar optics with a customizable working band. *Adv Quantum Technol* **6**, 2200153 (2023).
25. Barboza R, Bortolozzo U, Clerc MG et al. Berry phase of light under Bragg reflection by chiral liquid-crystal media. *Phys Rev Lett* **117**, 053903 (2016).
26. Kobashi J, Yoshida H, Ozaki M. Planar optics with patterned chiral liquid crystals. *Nat Photonics* **10**, 389–392 (2016).
27. Rafayelyan M, Tkachenko G, Brasselet E. Reflective spin-orbit geometric phase from chiral anisotropic optical media. *Phys Rev Lett* **116**, 253902 (2016).
28. Zheng ZG, Lu YQ, Li Q. Photoprogrammable mesogenic soft helical architectures: a promising avenue toward future chiro-optics. *Adv Mater* **32**, 1905318 (2020).
29. Xu CT, Liu BH, Peng C et al. Heliconical cholesterics endows spatial phase modulator with an electrically customizable working band. *Adv Opt Mater* **10**, 2201088 (2022).
30. Zhang YH, Chen P, Xu CT et al. Dynamically selective and simultaneous detection of spin and orbital angular momenta of light with thermoresponsive self-assembled chiral superstructures. *ACS Photonics* **9**, 1050–1057 (2022).
31. Zheng ZG, Hu HL, Zhang ZP et al. Digital photoprogramming of liquid-crystal superstructures featuring intrinsic chiral photoswitches. *Nat Photonics* **16**, 226–234 (2022).
32. Li SL, Chen ZY, Chen P et al. Geometric phase-encoded stimuli-responsive cholesteric liquid crystals for visualizing real-time remote monitoring: humidity sensing as a proof of concept. *Light Sci Appl* **13**, 27 (2024).
33. Gabor D. A new microscopic principle. *Nature* **161**, 777–778 (1948).
34. Gabor D. Holography, 1948-1971. *Science* **177**, 299–313 (1972).
35. Fang XY, Ren HR, Gu M. Orbital angular momentum holography for high-security encryption. *Nat Photonics* **14**, 102–108 (2019).
36. Gao H, Wang YX, Fan XH et al. Dynamic 3D meta-holography in visible range with large frame number and high frame rate. *Sci Adv* **6**, eaba8595 (2020).
37. Yang H, Ou K, Wan HY et al. Metasurface-empowered optical cryptography. *Mater Today* **67**, 424–445 (2023).
38. Liu YC, Xu K, Fan XH et al. Dynamic interactive bitwise meta-holography with ultra-high computational and display frame rates. *Opto-Electron Adv* **7**, 230108 (2024).
39. Kobashi J, Yoshida H, Ozaki M. Circularly-polarized, semitransparent and double-sided holograms based on helical photonic structures. *Sci Rep* **7**, 16470 (2017).
40. Liu SJ, Zhu L, Zhang YH et al. Bi-chiral nanostructures featuring dynamic optical rotatory dispersion for polychromatic light multiplexing. *Adv Mater* **35**, 2301714 (2023).
41. Kim J, Im JH, So S et al. Dynamic hyperspectral holography enabled by inverse-designed metasurfaces with oblique helicoidal cholesterics. *Adv Mater* **36**, 2311785 (2024).
42. Li KY, Wang YM, Pi DP et al. Multi-dimensional multiplexing optical secret sharing framework with cascaded liquid crystal holograms. *Opto-Electron Adv* **7**, 230121 (2024).
43. Zhu L, Liu SJ, Zhang YH et al. Light-addressable polychromatic holographic display via multi-encoded chiral superstructures. *Adv Funct Mater* **35**, 2507884 (2025).
44. Lee KM, Crenshaw EP, Rumi M et al. Effect of cell thickness on the electro-optic response of polymer stabilized cholesteric liquid crystals with negative dielectric anisotropy. *Materials* **13**, 746 (2020).
45. Lin JD, Zhang YS, Lee JY et al. Electrically tunable liquid-crystal–polymer composite laser with symmetric sandwich structure. *Macromolecules* **53**, 913–921 (2020).
46. Tondiglia VT, Natarajan LV, Bailey CA et al. Electrically induced bandwidth broadening in polymer stabilized cholesteric liquid crystals. *J Appl Phys* **110**, 053109 (2011).
47. Nemati H, Liu SY, Zola RS et al. Mechanism of electrically induced photonic band gap broadening in polymer stabilized cholesteric liquid crystals with negative dielectric anisotropies. *Soft Matter* **11**, 1208–1213 (2015).
48. Berreman DW. Optics in stratified and anisotropic media: 4×4-matrix formulation. *J Opt Soc Am B* **62**, 502–510 (1972).
49. Ma J, Zheng ZG, Liu YG et al. Electro-optical properties of polymer stabilized cholesteric liquid crystal film. *Chin Phys B* **20**, 024212 (2011).

50. Deng ZL, Jin MK, Ye X et al. Full-color complex-amplitude vectorial holograms based on multi-freedom metasurfaces. *Adv Funct Mater* **30**, 1910610 (2020).
51. Shan X, Li ZL, Dai Q et al. Metasurfaces with single-sized antennas for reconstructing full-color holographic images without cross talk. *Opt Lett* **46**, 5417–5420 (2021).
52. Yang ZJ, Huang PS, Lin YT et al. Asymmetric full-color vectorial meta-holograms empowered by pairs of exceptional points. *Nano Lett* **24**, 844–851 (2024).
53. Zhang DW, Xu CT, Chen QM et al. Cascaded chiral birefringent media enabled planar lens with programable chromatic aberration. *PhotoniX* **5**, 17 (2024).
54. Yuan R, Xu CT, Cao H et al. Spin-decoupled transflective spatial light modulations enabled by a piecewise-twisted anisotropic monolayer. *Adv Sci* **9**, 2202424 (2022).
55. Ren HR, Fang XY, Jang J et al. Complex-amplitude metasurface-based orbital angular momentum holography in momentum space. *Nat Nanotechnol* **15**, 948–955 (2020).
56. Xu CT, Zhang DW, Yuan R et al. Optical orbital angular momentum processors with electrically tailored working bands. *Laser Photonics Rev* **17**, 2201013 (2023).

Acknowledgements

We are grateful for financial supports from the National Key Research and Development Program of China (2022YFA1203700), the National Natural Science Foundation of China (NSFC) (T2488302, 62035008 and 62405129), the Natural Science Foundation of Jiangsu Province (BK20241197), and Fundamental Research Funds for the Central Universities (021314380244).

Author contributions

W. Hu conceived the original idea and designed the research. C. T. Xu and L. Li conducted the designs, fabricated the devices, and analyzed the data with the assistance of G. Y. Wang. C. T. Xu and Q. M. Chen performed the numerical calculations. C. T. Xu and W. Hu wrote the original manuscript. All the authors participated in the discussion and approved the manuscript. W. Hu supervised and directed the research.

Competing interests

The authors declare no competing financial interests.

Supplementary information

Supplementary information for this paper is available at https://doi.org/10.29026/oea.2026.250177

Published by Editorial Office of *Opto-Electronic Advance*, Institute of Optics and Electronics, Chinese Academy of Sciences.